Scientific Reports

https://doi.org/10.1038/s41598-026-44154-8

Article in Press

Rotary cutting tests and rock-breaking characteristics of triple-ridged PDC cutters in tight hard sandstones from Xujiahe Formation in Sichuan Basin in China

Received: 25 November 2025

Accepted: 10 March 2026

Published online: 31 March 2026

Cite this article as: He W., Li X., Zhang Z. *et al.* Rotary cutting tests and rock-breaking characteristics of triple-ridged PDC cutters in tight hard sandstones from Xujiahe Formation in Sichuan Basin in China. *Sci Rep* (2026). https://doi.org/10.1038/s41598-026-44154-8

Wenhao He, Xinlong Li, Zixin Zhang, Huaizhong Shi, Han Chen, Qijun Ma, Zhongwei Huang, Chao Xiong, Jiawen Dong & Yongxin Li

Rotary Cutting Tests and Rock-breaking Characteristics of Triple-ridged PDC Cutters in Tight Hard Sandstones from Xujiahe Formation in Sichuan Basin in China

Wenhao He [a,b*], Xinlong Li [a,b,c*], Zixin Zhang [a,b*], Huaizhong Shi [c✉], Han Chen [c], Qijun Ma [c], Zhongwei Huang [c✉], Chao Xiong [c✉], Jiawen Dong [a,b], Yongxin Li [a,b]

[a] *State Key Laboratory of Deep Geothermal Resources, China University of Petroleum-Beijing, Beijing, 102249, China;*

[b] *Beijing Key Laboratory of Oil and Gas Optical Detection Technology, China University of Petroleum-Beijing, Beijing, 102249, China;*

[c] *National Key Laboratory of Petroleum Resources and Engineering, China University of Petroleum-Beijing 102249, China.*

[*] *Authors with the same contribution.*

✉ *Authors to whom correspondence should be addressed: shz@cup.edu.cn (Huaizhong Shi), huangzw@cup.edu.cn (Zhongwei Huang), xiongc@cup.edu.cn (Chao Xiong)*

ABSTRACT: The Upper Triassic, particularly the Xujiahe Formation in the Sichuan Basin, exhibits significant exploration potential. However, reservoir characteristics such as low permeability, deep burial, and strong heterogeneity, limit the rock-breaking efficiency and service life of PDC bits. This study conducted experiments on the penetration and cutting of tight hard sandstone under drilling motion conditions, and compared the characteristics of triple-ridged PDC cutters (TRC) and planar PDC cutters (PLC) penetrating and cutting tight hard sandstone. Research results indicate that the optimal rock penetration effect is attained when the penetration angle of the PLC is 30° and that of the TRC is 25°. Under drilling motion conditions, the TRC exhibit superior stability during rock fragmentation and induce greater damage to the rock bottom. As the penetration velocity rises while the rotational speed drops, the extent of rock fragmentation diminishes; however, the fragmentation efficiency improves. Under these circumstances, the rock-breaking volume increases, and the

mechanical specific energy (MSE) decreases. In the process of drilling in highly abrasive sandstone formations, it is advisable to adopt high bit weight and medium - low rotational speed in engineering parameters. This research offers theoretical underpinnings for the design of drill bits and the selection of engineering parameters within highly abrasive formations.

Keywords: Tight hard sandstone, Triple-ridged PDC cutter, Rotary cutting , Hybrid-cutter PDC bit, Hybrid-cutter layout design

1. Introduction

Since the advent of the 21st century, conventional oil and gas exploration and development have entered their mid-to-late stages. Unconventional oil and gas resources, such as shale gas, shale oil, tight oil, and tight sandstone gas, have become the focal points of future exploration and development[1-3]. Among these, tight sandstone gas stands out as one of the more successfully developed unconventional resources domestically, accounting for one-fifth of China's natural gas production[3]. China boasts abundant tight sandstone gas resources, with the Xujiahe gas reservoirs in the Sichuan Basin being notable examples of successful development[4,5]. The Upper Triassic Xujiahe Formation in the Sichuan Basin is a key stratum for natural gas exploration, particularly due to its vast exploration potential. The reservoirs are characterized by their tightness, significant depth, strong heterogeneity, quartz content exceeding 85%, and rock hardness surpassing grade 7. These characteristics lead to severe drill bit wear, short drilling footage, frequent tripping, and a higher probability of gauge wear, presenting a series of engineering challenges[6-8].

As a pivotal factor in enhancing drilling speed in challenging formations, the performance of drill bits directly impacts drilling efficiency and operational costs. In recent years, PDC (Polycrystalline Diamond Compact) bits have experienced rapid development, with their drilling performance and variety substantially meeting the demands of oil and gas drilling. These bits now account for nearly 80% of the global oil and gas market share and over 90% of the total global drilling footage[9,10]. However, conventional PDC bits have shown limited effectiveness in addressing the complex challenges posed by unconventional drilling operations characterized by depth, thickness, hardness, and difficulty. In recent years, the widespread application of non-planar PDC

cutters has revolutionized the traditional single-shear rock-breaking mode of planar cutters. By employing a tensile-shear mechanism for efficient rock fragmentation, these innovative cutters have significantly enhanced impact resistance and wear resistance, thereby improving the rock-breaking efficiency and service life of PDC bits in deep and ultra-deep hard rock formations[11-13].

Current research methodologies on the rock-breaking mechanism of PDC cutters predominantly focus on theoretical modeling, numerical simulation, and cutting experiments. These approaches investigate rock-breaking characteristics such as the rock-breaking process, crack morphology[14], cuttings morphology[15], and groove morphology[16,17], as well as rock stress response, damage evolution characteristics[18], and cutter contact stress[19]. For instance, Souissi et al.[20] conducted penetration experiments on sandstone, limestone, and granite, comparing penetration energy, fracture morphology, and penetration force under various conditions. Huang et al.[21] employed the discrete element method to simulate the rock-breaking process of cutters, revealing a transition from ductile to brittle failure in rocks with increasing cutting depth. Che et al.[22] analyzed the rock-cutting process of PDC cutters using high-speed photography, observing the formation of a fan-shaped compacted core under shear and compressive stresses, followed by crack propagation to the rock surface and eventual large-scale chip detachment. Weiji Liu et al.[17] experimentally investigated the tensile-shear combined rock-breaking mechanism and groove characteristics of planar PDC cutters. In the study of non-conventional cutters, Xiong Chao[23-26] systematically investigated the rock-breaking mechanism of conical cutters, which primarily involve compaction crushing at the cutter tip and tensile fracture at the cutter front. To address the limited cutting area of conical cutters while retaining their high rock-breaking efficiency, ridge-shaped PDC cutters have gradually been introduced in oilfield applications. Among these non-conventional cutters, axe-shaped and triple-ridged PDC cutters are the most widely used. Researchers have conducted studies on the rock-breaking mechanisms of axe-shaped cutters, the rock-breaking characteristics of triple-ridged cutters, and the influence of the ridge structure of triple-ridged cutters on rock-breaking performance[27,28]. It has been found that triple-ridged cutters with a gentler ridge angle exhibit improved impact resistance[27], while their unique three-ridge structure increases the area of rock subjected to tensile and shear stresses, leading to greater volumetric fragmentation in brittle rocks[29].

In addition, some scholars have also studied the fragmentation behavior of rocks under mechanical action during the drilling process[30], exploring the mechanical response characteristics of rocks in drilling engineering[31], and found that rocks exhibit a transition from ductile to brittle failure under thermal shock[32]. It provides rich basis and reference for understanding the rock-breaking characteristics of PDC teeth under various motion modes.

In existing experimental and numerical simulation studies, the motion state of PDC cutters is typically simplified to linear or circular movements, without considering the actual motion patterns under real drilling conditions. Therefore, this study conducts experiments on the penetration and cutting of tight hard sandstone by triple-ridged PDC cutters under drilling motion conditions. It compares the characteristics of PDC cutters penetrating and cutting tight hard sandstone, providing theoretical support for the design of hybrid-cutters PDC bit and the optimization of drilling parameters in tight hard sandstone formations.

2. Rotary Cutting Experiment under Drilling Motion Conditions

2.1 Experimental Appratus and Sample Preparation

The rotary cutting rock-breaking experiment by PDC cutters was conducted using the high-temperature and high-pressure PDC cutter breaking and wear resistance testing system at China University of Petroleum (Beijing), as illustrated in Fig.1. The experimental apparatus comprises two main components: the cutting system and the control system. The cutting system, which was modified from a vertical lathe, includes a high-precision stepper motor, a rock sample holding device, a rotary table cutting base, a triaxial force sensor, a tool holding device, and a hydraulic pump. The control system consists of a programming system, a motion control system, and a data acquisition system. This setup enables the testing of single and multiple PDC cutter wear resistance, rotary rock breaking, and linear rock breaking. It also facilitates the monitoring of the rock breaking process through the use of infrared thermometer and high-speed photography. The rock sample holding capacity is up to 500*500*500 mm, with the rotary table speed ranging from 38 to 170 rpm. The cutting speed (The velocity in the cutting direction during the linear motion of PDC cutters) is adjustable from 10 to 500 mm/s, and the overall displacement adjustment precision is 0.001 mm. The triaxial force acquisition frequency ranges from 0 to 3000 Hz. The experimental equipment

provides pressure through a bidirectional hydraulic pump to simulate the formation confining pressure, and can heat the rock through a muffle furnace to simulate high - temperature conditions. However, the experimental conditions implemented in this study are more focused on simulating the motion state of the PDC cutters during the drilling process of the PDC bit, rather than emphasizing the simulation of environmental conditions. Therefore, the experiment was conducted at room temperature. The hydraulic pump provided a bidirectional clamping force of approximately 10 MPa to secure the rock.

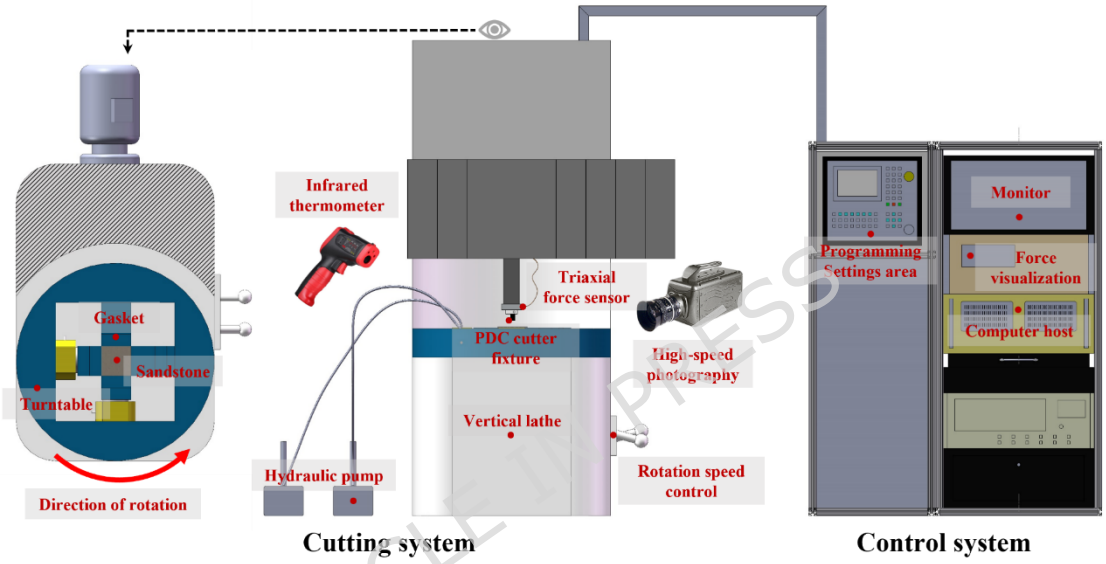

Fig.1 Rock-breaking experimental system of PDC cutter

The parameters of the triple-ridged PDC cutters (TRC) and the planar PDC cutter (PLC) used in this study are shown in Fig.2 (a), (b), respectively. Fig.2 (c) exhibits the tight hard sandstones used in the research. The rock sample utilized in this experiment is a rectangular tight hard sandstone with a length and width of 300 mm and a height of 130 mm, which can be collected from the outcrops in Xujiahe Formation, Sichuan Basin. The detailed mechanical parameters of the sample were obtained from confined compression tests, as shown in Table 1.

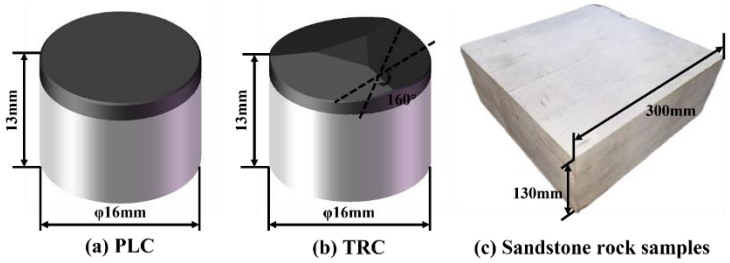

Fig.2 The geometrical parameter of PDC cutters and sandstone samples

Table 1 Basic mechanical properties of sandstone samples

Properties	Density (g/cm^3)	Young's modulus (GPa)	UCS (MPa)	Poisson's ratio	Tensile strength (MPa)
Avg	2.435	30.61	197.01	0.219	11.67

Note: The properties were tested three times.

The process of the experiment implementation is shown in Fig.3. The experiment is carried out in accordance with the following steps:

(1) Prior to the experiment, put on protective equipment and conduct a safety inspection to ensure the testing apparatus is functioning properly.

(2) Prepare experimental materials, including rock samples, PDC cutters, fixtures, sieves net, and an electronic scale.

(3) According to the experimental protocol, select the appropriate fixture and PDC cutter, secure the PDC cutter and rock sample, and perform leveling calibration. Based on the experimental principles, program the cutting parameters such as rotation radius, penetration velocity, and rotational speed on the programming interface.

(4) Execute the program, set the parameters for the data acquisition system (with a force sampling frequency of 500 fps in this experiment), measure and record the force data. Collect rock cuttings during the experiment and save the experimental data to conclude this set of experiments.

(5) Clean the equipment, adjust the parameters, and repeat the experimental procedure to complete all experiments.

(6) After the cutting experiment, sieve the rock cuttings using 10-mesh (2 mm), 20-mesh (0.84 mm), 30-mesh (0.59 mm), and 80-mesh (0.177 mm) sieves. Weigh the sieved cuttings using an electronic balance (with a precision of 0.01 g) and scan the post-experiment rock surface using a RigelScan scanner to complete the post-processing tasks.

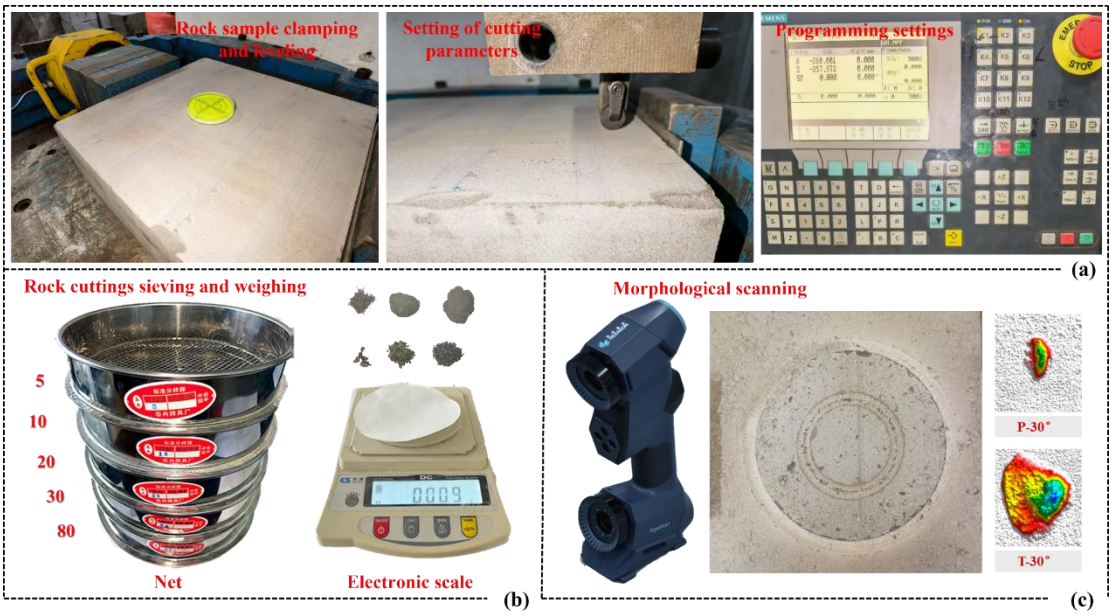

Fig.3 Experimental procedures and experimental treatments

2.2 Experimental Design

During the drilling process, the PDC cutters on the PDC bit move downward under the action of the weight of bit (WOB) and simultaneously rotate along with the bit. The schematic diagram illustrating the experimental principle is presented in Fig.4. Throughout the experimental process, the sandstone sample is secured on the rotating platform and undergoes counterclockwise rotation, whereas the PDC cutter is clamped onto the equipment and undergo uniform axial motion therewith. The rotation of the rock sample is synchronized with the downward movement of the PDC cutter, thereby simulating the motion state of the PDC cutter during drilling operations. This is not a fixed cutting depth. The cutting depth of the PDC cutter continuously increases from 0 to 6 mm during the motion process. The rotation radius (r), axial penetration velocity (v), and rotational speed (n) of the PDC cutter are precisely configured, with the center point of the PDC cutter positioned on the XOZ plane to eliminate the influence of lateral angles on the force distribution of the PDC cutter. In the penetration experiments, only axial motion was configured. The three-axis forces acting on the PDC cutters include the axial force F_z, the tangential force F_y, and the lateral force F_x.

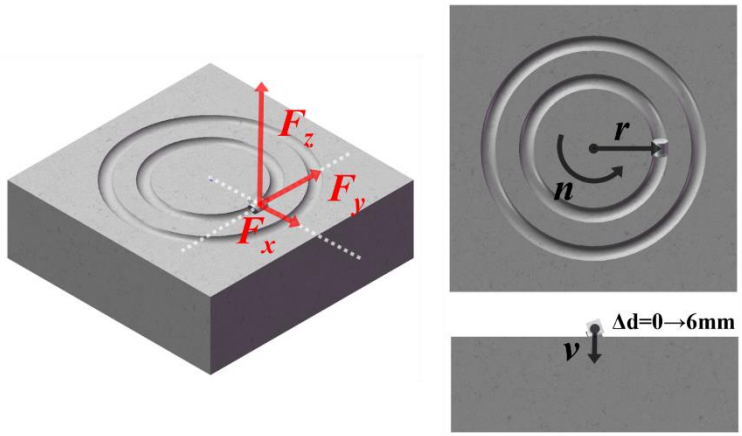

Fig.4 Schematic diagram of the principle of experiment

The penetration experiment scheme and the rock-breaking experiment scheme adopted in the research are respectively shown in Table 2 and Table 3.

As shown in Table 2, the penetration experiment of PDC cutters in tight hard sandstone was set up with a total of 30 groups of experiments, including different penetration velocity and different penetration angles for the TRC and the PLC. The total penetration depth of the PDC cutters was set at 3.5 mm and this is determined based on the exposure height of the PDC cutters on the PDC bit[33].

Table 2 The penetration experimental scheme of PDC cutters in tight hard sandstone

Number	PDC cutter	Penetration velocity (mm/s)	Penetration angle (°)
1~11	PLC	0.8	5/10/15/20/25/30/35/40/45/50/55
12~15	PLC	0.4/0.6/1.0/1.2	15
16~26	TRC	0.8	5/10/15/20/25/30/35/40/45/50/55
27~30	TRC	0.4/0.6/1.0/1.2	15

Note: The total penetration depth is set at 3.5 mm.

The rotary cutting experimental scheme of PDC cutters in tight hard sandstone shown in Table 3 were conducted with different penetration velocity (v), rotation radius (r) and rotational speeds (n) for both TRC and PLC, totaling 26 groups. Considering the structural features of the 8 1/2" PDC bits, the rotation radius of 50, 70, 90 and 110 mm respectively represent the inner cone, nose, outer cone and gauge of the PDC bit. The different rotational speeds represent the rotational speeds of the PDC bit during the drilling process, while the penetration velocity denote the rate of penetration (ROP) of the PDC bit in drilling operations. Under the experimental conditions, the equivalent ROP ranged from 1.44 to 4.32 m/h. The equivalent ROP referenced herein is derived through the conversion of penetration velocity, specifically involving unit transformation between millimeters per second (mm/s) and meters per hour (m/h). Throughout the entire process, the maximum axial

displacement of the PDC cutter was 6 mm.

Table 3 The rotary cutting experimental scheme of PDC cutters in tight hard sandstone

Number	PDC cutter	Penetration velocity (mm/s)	Rotation radius (mm)	Rotational speed (rpm)
1~5	PLC	0.4/0.6/0.8/1.0/1.2	70	76
6~9	PLC	0.8	30/50/90/110	76
10~13	PLC	0.8	70	38/65/85/130
14~18	TRC	0.4/0.6/0.8/1.0/1.2	70	76
19~22	TRC	0.8	30/50/90/110	76
23~36	TRC	0.8	70	38/65/85/130

Note: The axial movement range of the PDC cutter is 0 to 6 mm.

2.3 Data processing

2.6.1 Standard error of the estimate

The standard error of the estimate (SEE) quantifies the average deviation of data points from the regression line, with its unit consistent with that of the dependent variable (Y). By performing linear regression on the experimentally obtained tangential and axial force data and calculating the residual standard error of the data points, we can characterize the fluctuation level of the mechanical data. A smaller SEE indicates that the data points are closer to the fitted curve, suggesting lower fluctuation and consequently greater stability in the cutting process. The computational methodology for determining the residual standard error is as follows:

$$SEE = \sqrt{\frac{\sum(y_i - \hat{y}_i)^2}{n-2}} \tag{1}$$

In the Equation, y_i represents the observed value, $\hat{y}_i$ represents the predicted value, n represents the number of data points.

2.6.2 Mechanical specific energy

The energy consumption for rock fragmentation is an important indicator for measuring drilling efficiency. In rock fragmentation science, the mechanical specific energy (MSE) for rock breaking reflects the efficiency of rock fragmentation from an energy perspective[34]. It is defined as the energy consumption required for the fragmentation of a unit volume of rock. The MSE can be expressed as：

$$MSE = \frac{W}{V} \tag{2}$$

In the Equation, W represents the energy consumed for rock fragmentation, and V represents the volume of rock-breaking, which can be directly obtained by scanning the morphology

of the cutting slot in this study.

During this experiment, the tangential force and axial force were used to break the rock and do work. The direct acquisition of the mechanical data (F) and the corresponding relationship with time (t) in the experiment is shown in Fig.5 (a). It is evident that both the tangential force F_y and the axial force F_z exhibit a linear increasing trend with time. To calculate the work performed, it is necessary to transform the data into the relationship between force (F) and relative displacement (L).

In the axial direction, the PDC cutter exhibits uniform downward motion, yielding the following relationship:

$$L_z = v * t \tag{3}$$

In the Equation, v represents the penetration velocity, mm/s.

And in the tangential direction, the PDC cutter and the rock have a relative rotational motion, and thus:

$$L_y = v_y * t = \omega * r * t = \frac{2\pi * n * r * t}{60} \tag{4}$$

In the Equation, v_y represents the linear velocity, mm/s, ω represents the angular velocity; n represents the rotational speed, revolutions per minute (rpm); and r indicates the radius of rotation, mm.

According to Equations (2) to (4), the expression of MSE is shown in Equation (5). The areas S_y and S_z in Fig.5 (b) and (c) are calculated by the integration method, representing the work done by the tangential force and the axial force respectively.

$$MSE = \frac{W}{V} = \frac{W_y + W_z}{V} = \frac{\int_0^{Ly} F_y dx + \int_0^{Lz} F_z dx}{V} \tag{5}$$

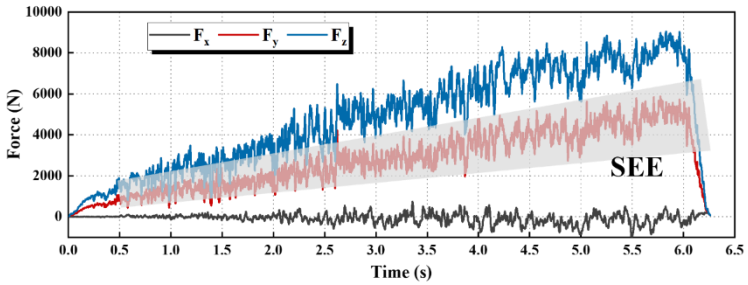

(a) Force analysis of PDC cutters during rock-Cutting experiments

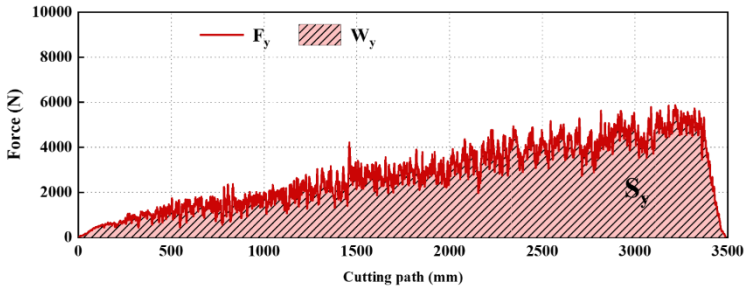

(b) The tangential force F_y and work calculation

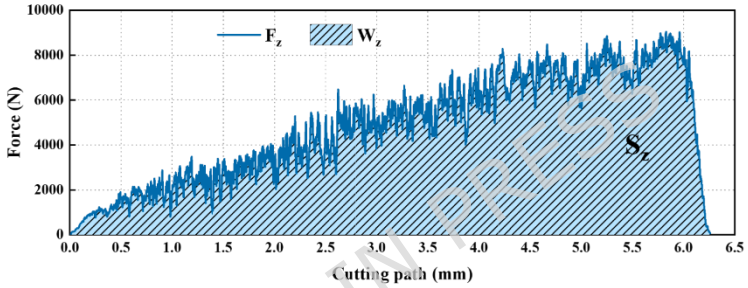

(c) The axial force F_z and work calculation

Fig.5 Force data and processing methods of rotary cutting experiment

2.6.3 Fractal dimension and maximum size of rock cuttings

Fractal theory is a mathematical scientific framework employed to delineate the self-similarity and scale invariance of systems, constituting a pivotal branch within contemporary nonlinear science[35]. It serves as a crucial mathematical instrument and methodology in scientific research, with pertinent studies and applications in rock fragmentation[36,37]. The relationship between the fractal dimension of rock debris and the mass fraction can be expressed as[38]:

$$ln\frac{M_L}{M_T} = (3 - D_l)\,ln(l) - (3 - D_l)\,ln(l_{max}) \tag{6}$$

Among them, M_L represents the accumulative mass of rock cuttings smaller than size l, M_T represents the total mass of rock cuttings, D_l represents the fractal dimension of rock cuttings, l represents the size of rock cuttings, and l_{max} represents the maximum size of rock cuttings.

3. Results and analysis

3.1 Penetration characteristics of PDC cutters

3.1.1 The penetration force and topography of crushed pit

Fig.6 illustrates the penetration force (axial force) curves during the penetration experiment under various experimental conditions. Within the tested range, the penetration force consistently exhibited a continuous loading-fluctuation-loading trend until the penetration depth reached the preset value of 3.5 mm, at which point the penetration force attained its maximum value, defined as the ultimate penetration force. Prior to reaching the ultimate limit of penetration depth, the fluctuation range of the penetration force can reflect the degree of brittle failure. For example, under the condition of 30°, the brittle failure mode of TRC under the 30° condition is more prominent than that of PLC. The results presented in Fig.7 also serve to validate this viewpoint. The Fig.6 demonstrates that the rate of increase in penetration force accelerates progressively with greater penetration depth. Furthermore, the force curve for the TRC consistently remains above that of the PLC, indicating that greater penetration force is required for the TRC at equivalent penetration depths, a phenomenon attributable to the prismatic structure of the TRC. The special ridge structure of the TRC increases the contact area with the rock during intrusion.

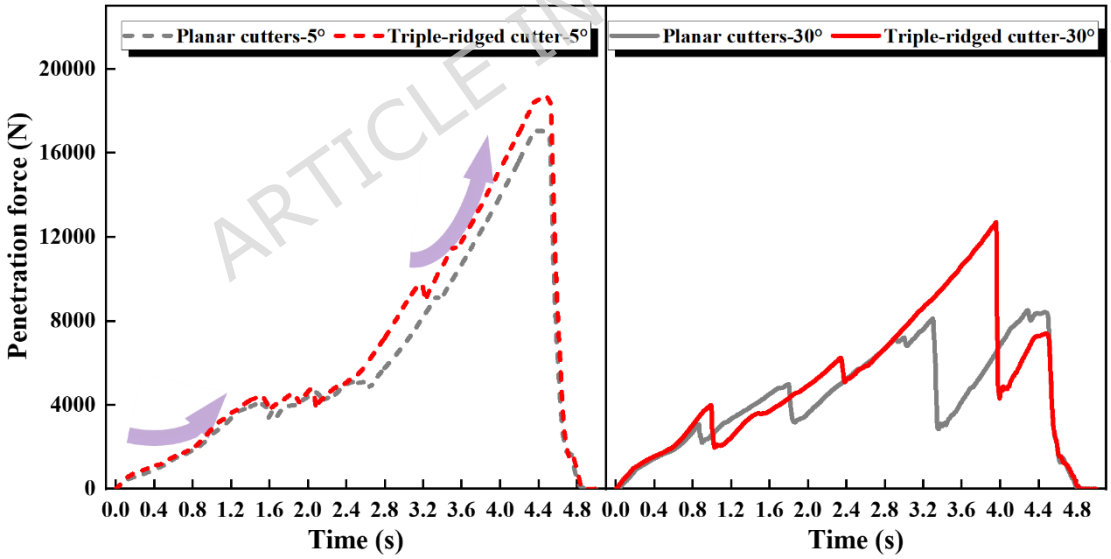

Fig.6 Penetration force curves under different experimental conditions

Fig.7 illustrates the topography of crushed pits formed by PDC cutters during the penetration into rock under various experimental conditions. Based on the corresponding mechanical data and graphical analysis, we observed a continuous loading-fluctuation-loading trend in the penetration force, which corresponds to the stages of elastic deformation, brittle failure, and elastic deformation of the rock. The characteristics of the crushed pits exhibit significant variations at different

penetration angles, with greater force fluctuations correlating to more extensive brittle failure zones. Optimal design of the PDC cutter angles on the drill bit facilitates enhanced rock penetration efficiency under identical weight-on-bit conditions.

The total penetration depth in penetration experiments is set at 3.5 mm. Post-experiment analysis revealed that the crushed pits depth ranged from 0 to 1.8 mm. During the final stage of the penetration process, although the penetration force increased, it was not accompanied by rock failure. The terminal crater depth remained essentially consistent with the depth at which the last brittle failure occurred. This indicates that in drilling operations, there exists a critical weight-on-bit value at which the PDC cutter's penetration into the rock maximizes the extent of rock damage, thereby optimizing rock-breaking efficiency. After the initial damage, continuously increasing the WOB will still cause damage to the rock, but this is a phased process, that is, the PDC cutter first compacts and then breaks the rock. Before reaching the critical value of rock breaking, it can be understood that the rock undergoes elastic deformation under the extrusion effect and returns to its original state after unloading.

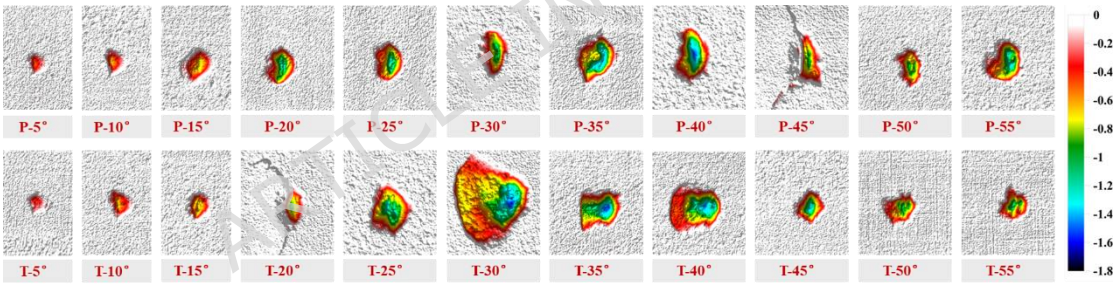

(a) The topography of crushed pits under different penetration angles

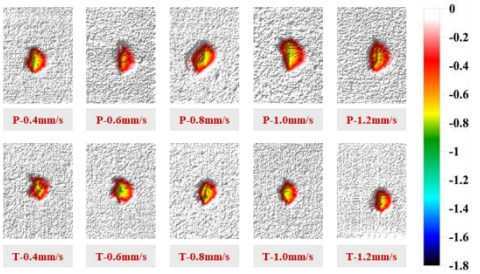

(b) The topography of crushed pits under different penetration velocities

Fig.7 The topography of crushed pits under different conditions obtained by the scanner

3.1.2 The ultimate penetration force model

The data points of ultimate penetration force under varying conditions are plotted in Fig.8, with the data points fitted using both sine and linear functions. As illustrated in Fig.8 (a), within the tested

range, the ultimate penetration force at a penetration depth of 3.5 mm initially decreases and subsequently increases with the rise in cutting angle, reaching its minimum at a PLC penetration angle of 30° and a TRC penetration angle of 25°. Fig.8 (b) demonstrates that within the tested range, the ultimate penetration force for the TRC at a penetration depth of 3.5 mm exceeds that of the PLC, with both exhibiting a consistent slight increase as the penetration velocity escalates. The derived models are presented in Equations (7) to (10).

$$F_p = 12593.68 + 4743.09 * \sin[\pi\,(\alpha + 8.35)/26.36] \quad R^2 = 0.952 \tag{7}$$

$$F_T = 16114.91 + 3686.13 * sin[\pi\,(\alpha + 21.94)/34.89] \quad R^2 = 0.902 \tag{8}$$

$$F_p = 12550.58 + 2197.42 * v \quad R^2 = 0.976 \tag{9}$$

$$F_T = 12622.42 + 2589.38 * v \quad R^2 = 0.938 \tag{10}$$

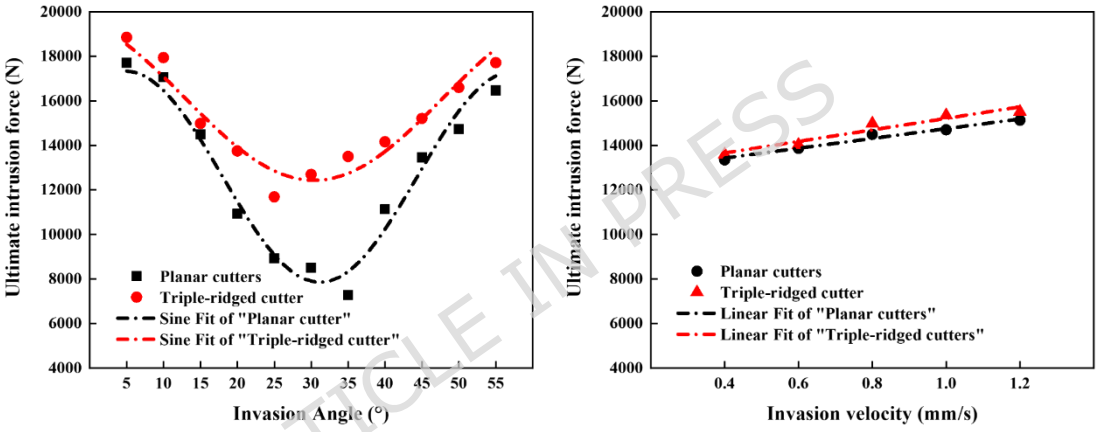

(a) The variation pattern of ultimate penetration force with invasion angle

(b) The variation pattern of ultimate penetration force with invasion velocity

Fig.8 Ultimate penetration force and model

3.2 Rock-breaking Characteristics of PDC cutters

3.2.1 Triaxial force

As illustrated in Fig.9, the triaxial force distribution of PDC cutter under varying penetration velocity is presented, where the triaxial forces are denoted as F_x, F_y, and F_z. During the cutting process, the PDC cutter remains stationary without any displacement in the x-direction, resulting in a negligible lateral force F_x, which is excluded from the analysis. The tangential force F_y represents the cutting force in the direction of the PDC cutter's movement, corresponding to the torque in the drilling process. The axial force F_z is the vertical force required for the PDC cutter to penetrate the rock, corresponding to the weight on bit in the drilling process.

In the experiment, the axial movement range of the PDC cutter is 0 to 6 mm. From the Fig.9, it is evident that both the tangential force F_y and the axial force F_z exhibit a linear increasing trend with time, accompanied by continuous fluctuations. On one hand, in this experiment, the continuous downward displacement of the PDC cutter is fixed, which means the contact area continuously increases. This also corresponds to the continuous increase in both the axial force required for intrusive rock and the cutting force required for rock cutting. On the other hand, the total penetration depth has not reached the critical value at which the PDC cutter is fully embedded in the rock (i.e., the radius of the cutter - 8 mm). Consequently, linear fitting methods are applied to F_y and F_z, where the slope of the fitted line indicates the rate of force change per unit time. Additionally, the SEE is introduced to characterize the stability of the rock-breaking process during cutting.

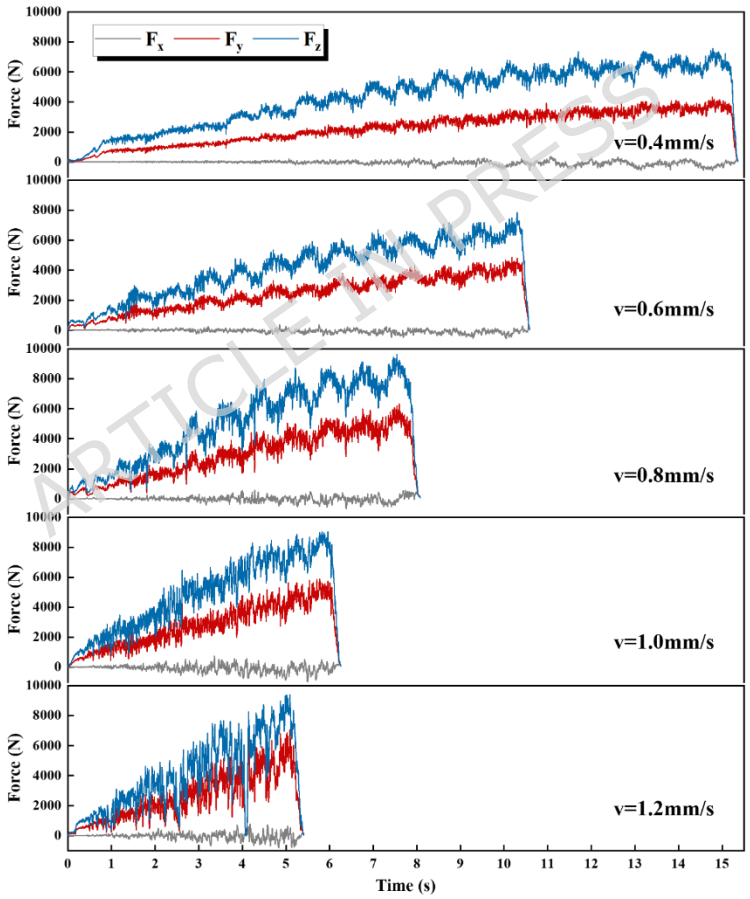

Fig.9 Triaxial force curves of TRC under different penetration velocities (G14~G18)

The slope of the fitted linear regression in the mechanical data represents the rate of force variation per unit time. As illustrated in Fig.10 (a), the ratio of slope to penetration velocity yields the mean value. It can be computed that for every 1 - millimeter increment in the cutting depth of

PDC cutters, the tangential force of PLC rises by 763 N, and the axial force increases by 1509 N. In the case of TRC, the tangential force increases by 620 N, and the axial force increases by 1121 N. Fig.10 (b) demonstrates that variations in rotation radius have negligible impact on the force per unit depth of PDC cutters. Fig.10 (c) reveals that higher rotational speeds result in greater forces on PDC cutters, while the rate of force variation per unit time progressively decreases.

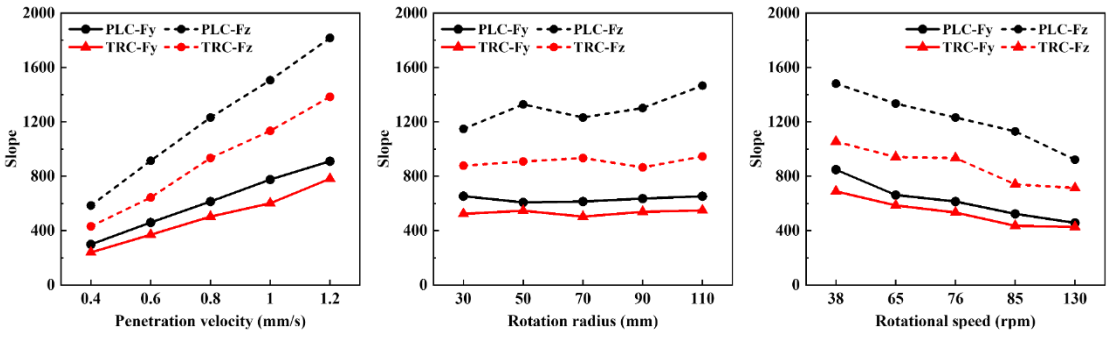

(a) The variation pattern of Slope with penetration velocity

(b) The variation pattern of Slope with rotation radius

(c) The variation pattern of Slope with rotational speed

Fig.10 The variation pattern of slope with cutting parameters

Fig.11 illustrates the variation pattern of the SEE with cutting parameters. It can be observed that lower penetration velocity and higher rotational speeds result in reduced SEE values, indicating enhanced stability in forces and smoother drilling processes. Conversely, With the increase in the penetration velocity, the cutting depth of the PDC cutters is correspondingly greater, which validates the observation of more pronounced fluctuations during the cutting process. Elevated rotational speeds increase the contact frequency between cutters and rock formations, thereby mitigating force fluctuations caused by rotational instability or vibrations during the cutting process. The rotation radius exhibits minimal influence on the results, demonstrating no significant pattern. Furthermore, under various experimental conditions, the SEE for the TRC consistently remain lower than those of the PLC.

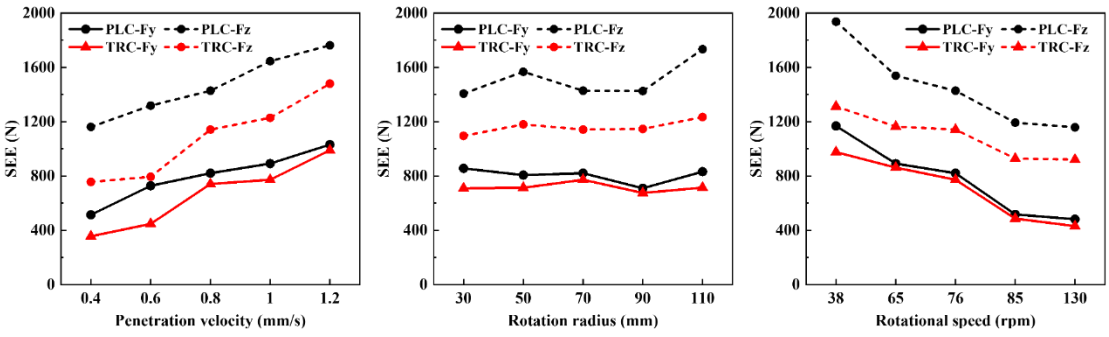

(a) The variation pattern of SEE with penetration velocity

(b) The variation pattern of SEE with rotation radius

(c) The variation pattern of SEE with rotational speed

Fig.11 The variation pattern of SEE with cutting parameters

3.2.2 Topography of cutting grooves

The topography scanning of the cutting grooves post-machining experiments yielded the groove profiles under various conditions, as illustrated in Fig.12. According to Fig.12 (a) and (b), the analysis reveals that higher penetration velocities and lower rotational speeds result in more pronounced lateral expansion of the groove surfaces. This phenomenon can likewise be attributed to the increase in the relative cutting depth of PDC cutters. The TRC exhibit significantly larger limit depth regions and induce greater propagation damage to the rock substrate.

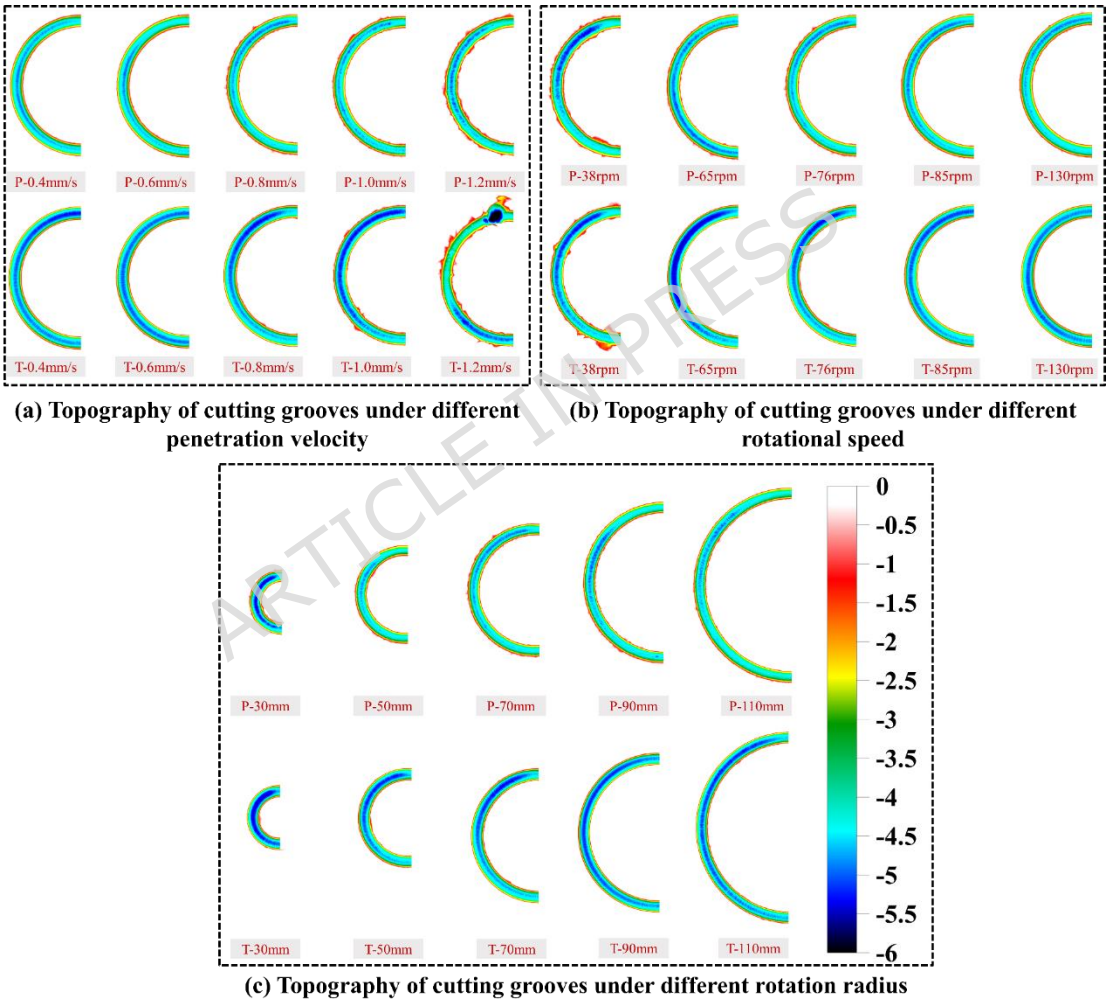

(a) Topography of cutting grooves under different penetration velocity

(b) Topography of cutting grooves under different rotational speed

(c) Topography of cutting grooves under different rotation radius

Fig.12 Topography of cutting grooves under different conditions

3.2.3 Fractal characteristics of rock cuttings

The cuttings collected from each group of cutting experiments were sieved and weighed, with the mass percentages of cuttings of different sizes illustrated in Fig.13. Cuttings larger than 10 mesh

(2 mm) were classified as large cuttings. The measurement results indicate that the proportion of large cuttings increases with higher penetration velocity, while higher rotational speeds result in a lower proportion of large cuttings, with the cutting process predominantly producing powdered cuttings. The influence of rotation radius on the mass distribution of cuttings is minimal, showing negligible variation across different radius. Additionally, under identical conditions, the proportion of large cuttings generated by TRC is greater than that produced by PLC.

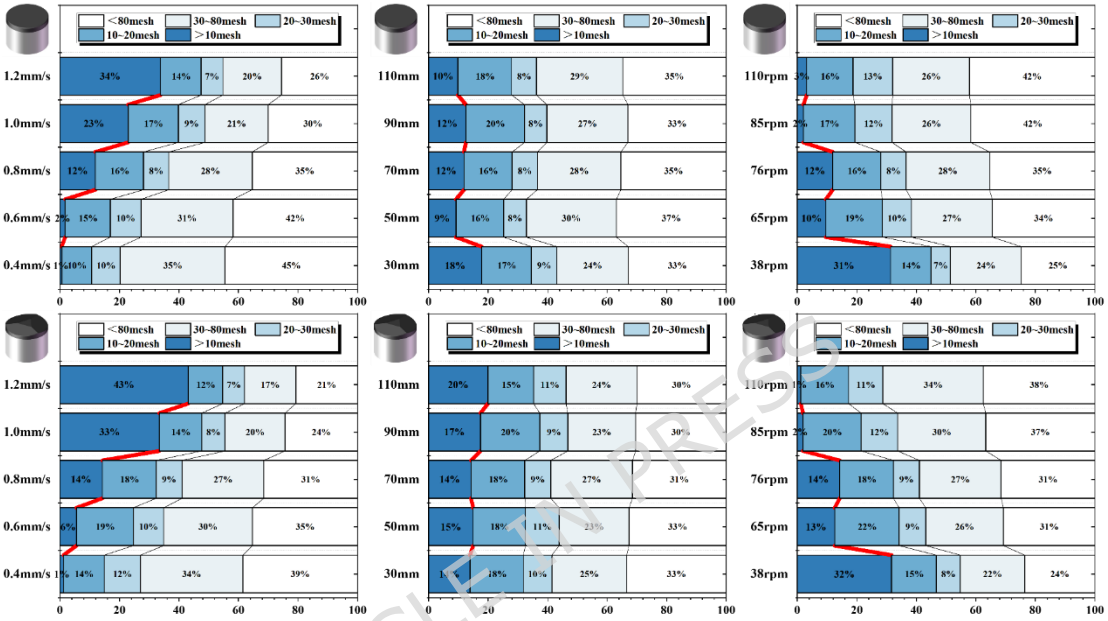

Fig.13 The mass proportion of rock cuttings of different sizes

According to the method introduced in Section 2.6.3 Fractal dimension and maximum size of rock cuttings, the fractal dimension and the maximum size of rock cuttings under different conditions were calculated, and their variations with cutting parameters are shown in Fig.14. The fractal dimension quantitatively describes the degree of rock fragmentation, indicating that the higher the degree of fragmentation, the larger the fractal dimension value. As shown in Fig.14, the fractal dimension of rock cuttings always remains within the range of 2 to 3, that is, a parameter between two-dimensional and three-dimensional is used to describe the degree of rock fragmentation. When more large rock cuttings are produced, in the spatial dimension, the shape of the rock cuttings tends to be more like the surface form of large rock cuttings rather than the three-dimensional form of granular and powdered rock cuttings. At this time, the fractal dimension is closer to 2 and thus decreases. The fractal dimension of the TRC is always smaller than that of the

PLC, while the maximum size of the rock cuttings is always larger than that of the PLC, indicating that the TRC have a lower degree of rock fragmentation but a higher rock-breaking efficiency.

From Fig.14 (a), we find that as the penetration velocity increases, the fractal dimension of cuttings decreases, while the maximum size of cuttings keeps rising. When the ROP increases during drilling operations, it generally corresponds to a higher drilling pressure, and the single penetration depth of PDC cutters is deeper. At this time, the degree of rock fragmentation decreases, resulting in larger-sized cuttings and higher rock-breaking efficiency. Fig.14 (b) shows that the rotation radius has a relatively small impact on the fractal characteristics of cuttings, and there is no difference in the size of cuttings produced by different parts of the drill bit during cutting and rock fragmentation. In Fig.14 (c), we can see that as the rotational speed increases, the fractal dimension keeps rising, while the maximum size of cuttings keeps decreasing. Moreover, as the rotational speed becomes higher and higher, the response degree becomes smaller and smaller. A high rotational speed can increase the contact frequency between PDC cutters and rocks, leading to a higher degree of rock fragmentation, but it is also accompanied by a decrease in rock-breaking efficiency.

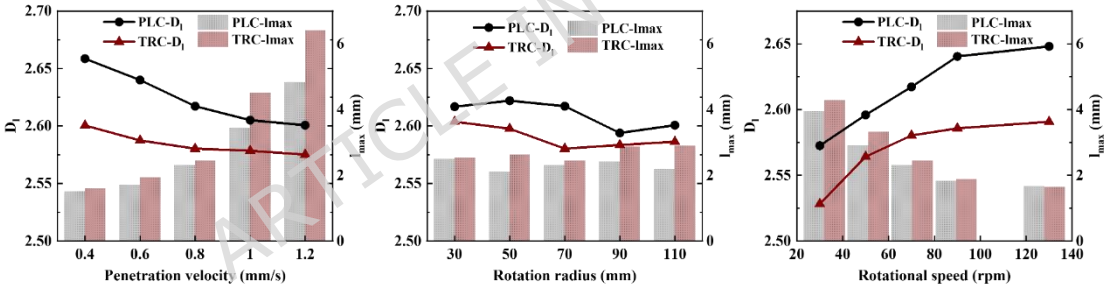

(a) The variation pattern of D_l and l_{max} with penetration velocity

(b) The variation pattern of D_l and l_{max} with rotation radius

(c) The variation pattern of D_l and l_{max} with rotational speed

Fig.14 The variation of fractal dimension and maximum cutting size with cutting parameters

3.2.4 Rock-breaking volume and MSE

According to the method introduced in Section 2.6.2 Mechanical specific energy, the MSE under different conditions was calculated. The variations of the rock-breaking volume, work done, and MSE of PDC cutters under different cutting conditions are shown in Fig.15. It is found that the rock-breaking volume of the PLC is always less than that of the TRC, while the work done by the axial force and tangential force is always greater than that of the TRC, resulting in a higher MSE for the PLC than the TRC. That is, from the perspective of MSE, under the simulated drilling conditions, the rock-breaking efficiency of the TRC is higher than that of the PLC. An increase in

penetration velocity leads to a larger rock-breaking volume by PDC cutters, resulting in a lower mechanical specific energy (MSE); conversely, higher rotational speed reduces the rock-breaking volume of PDC cutters, causing an increase in MSE.

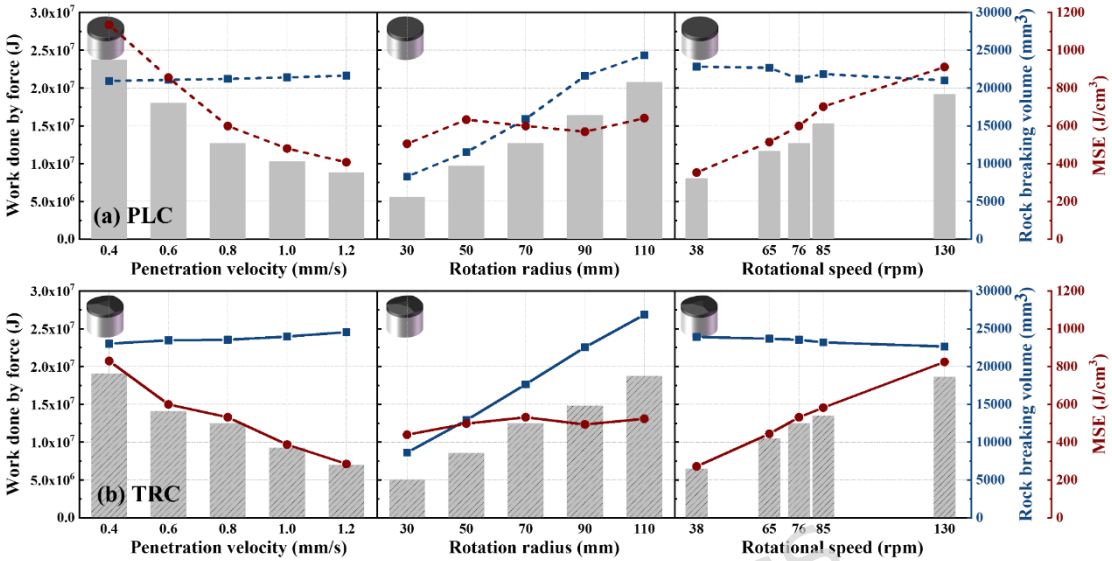

Fig.15 The variation of rock-breaking volume and MSE with cutting parameters

The statistical analysis of the work performed by axial and tangential forces during the cutting process, as illustrated in Fig.16, reveals that under simulated drilling conditions, the work done by axial forces in rock breaking remains consistent across various experimental conditions. Notably, the work performed by axial forces in rock fragmentation is significantly smaller compared to that of tangential forces, differing by approximately three orders of magnitude. Consequently, the impact of axial forces on specific energy consumption for rock breaking is negligible. The axial force work and tangential force work of the TCR are both less than those of the PLC.

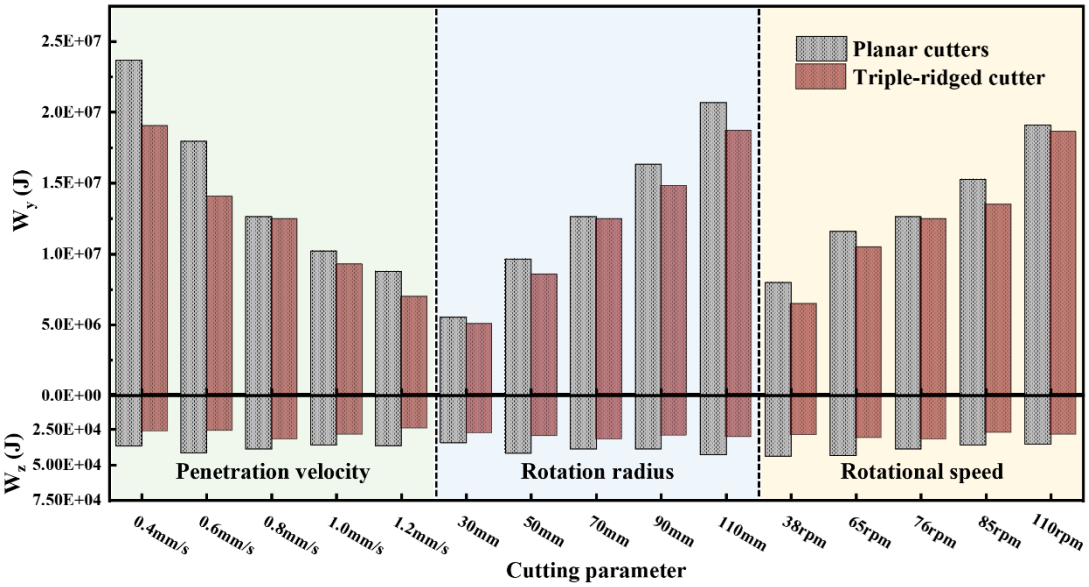

Fig.16 Axial force and tangential force work in the cutting process

4. Conclusions

In this study, experiments on PDC cutters penetration into tight hard sandstone were carried out, and experiments on breaking tight hard sandstone with triple-ridged PDC cutters (TRC) and planar PDC cutter (PLC) were conducted under simulated drilling conditions. The characteristics of PDC cutters penetration and cutting tight hard sandstone were analyzed. The main conclusions obtained include:

(1) A continuous loading-fluctuation-loading trend in the penetration force, which corresponds to the stages of elastic deformation, brittle failure, and elastic deformation of the rock. The fluctuation degree of the penetration force is positively correlated with the range of brittle failure.

(2) Under identical penetration depths, the TRC requires a greater penetration force. Optimal rock penetration is achieved at a penetration angle of 30° for PLC and 25° for TRC. And a mathematical model correlating the ultimate penetration force with the penetration angle has been established.

(3) Under simulated drilling conditions, for every 1 - millimeter increment in the cutting depth of the PDC cutters, the tangential force acting on the PLC increases by 763 N, and the axial force increases by 1509 N. Meanwhile, for the TCR, the tangential force increases by 620 N, and the axial force increases by 1121 N. The TRC exhibit superior stability during rock fragmentation and induce greater damage to the rock bottom.

(4) A faster penetration velocity and a lower rotational speed result in more pronounced expansion on the cut groove surface. The maximum size of rock cuttings generated increases, along with greater fluctuation in cutting forces. The fractal dimension of rock cuttings decreases, indicating a reduced degree of rock fragmentation and higher rock fragmentation efficiency.

(5) Under simulated drilling conditions, TRC exhibits higher rock-breaking efficiency than PLC. Higher penetration velocity with lower rotational speeds increase rock-breaking volume while reducing MSE. For strongly abrasive sandstone formations, engineering parameters featuring high bit weight and medium-low rotational speeds are recommended.

5. Funding details

This research is supported by Natural Science Foundation of China Grant (No.U24B6001) , General Program of National Natural Science Foundation of China Grant (No. 52274016), the Foundation of State Key Laboratory of Petroleum Resources and Prospecting Grant (PRE/DX-2402).

6. Data availability

All data supporting the findings of this study are available within the paper.

References

1. He, X. P. et al. Challenges and countermeasures for beneficial development of unconventional oil and gas resources in China. Chin. Pet. Explor. 30, 26 (2025).
2. Radwan, A. E., Yin, S. & Li, H. H. Petroleum geology of conventional and unconventional resources: Introduction. Geol. J. 58, 3965-3969 (2023).
3. Xu, X. H., Zhou, Z. M., Song, Z. X. & Yang, G. Q. Methods and key parameters for oil and gas resource assessment and distribution characteristics of oil and gas resource: a case study of resource assessment of SINOPEC during the 13th Five-Year Plan period. Pet. Geol. Exp. 45, 832-843 (2023).
4. Song, F., Kong, Q., Su, N., Jiao, G. & Xu, M. Formation mechanism of the upper Paleozoic tight sandstone gas reservoir in the Daniudi gas field, Ordos Basin, China. Front. Earth Sci. 12, 1355494 (2024).
5. Shusheng, G. et al. Research on the basic theory and application of enhanced recovery in tight sandstone gas reservoirs. Heliyon 11, e41306 (2025).

6. Wu, D. et al. Study on Reservoir Characteristics, the Tightening Process and Reservoir Quality in Source-to-Sink Systems in the Xu-2 Member of the Xujiahe Formation in the Western Sichuan Basin, Western China. Minerals 15, 625 (2025).
7. Wu, D., Yu, Y., Lin, L., Chen, H. & Liu, S. Characteristics and Control Factors of a High-Quality Deeply Buried Calcareous Sandstone Reservoir, the Fourth Member of the Upper Xujiahe Formation in the Western Sichuan Basin, China. Minerals 14, 872 (2024).
8. Wen, L. et al. New exploration fields and resource potential of continental tight oil and gas in Sichuan Basin. Acta Pet. Sin. 46, 77 (2025).
9. Liao, Q. et al. Study on Different Kinds of Drill Bits and Their Usage in Hard-to-Drill Formations. Chem. Technol. Fuels Oils 59, 783-790 (2023).
10. Luo, X. & Gou, R. Friction and Wear of Polycrystalline Diamond in Oil Drilling: A Review. Fuller. Nanotub. Carbon Nanostruct. 33, 473-486 (2025).
11. Zhang, C. et al. Numerical simulation and experimental study on the interaction between a convex ring PDC bit and rock. Geoenergy Sci. Eng. 230, 212247 (2023).
12. Guo, F. et al. Failure mechanism and lessons from two-wing polycrystalline diamond compact drill bit drilling in coal roadways. Eng. Fail. Anal. 168, 109089 (2025).
13. Ke, X. et al. Cutting mechanism of a special 3D concave-shaped PDC cutter applicable to the Weiyuan shale. J. Pet. Explor. Prod. Technol. 13, 1435-1451 (2023).
14. Cheng, Z. et al. Imaging the formation process of cuttings: characteristics of cuttings and mechanical specific energy in single PDC cutter tests. J. Pet. Sci. Eng. 171, 854-862 (2018).
15. Zhu, X., Hu, H., Liu, W., Li, R. & Wen, X. Rock fragmentation mechanism of PDC cutter from the insight of cutting chips. Geoenergy Sci. Eng. 240, 213001 (2024).
16. Rong, Z. et al. Experimental and theoretical analysis of rock failure characteristics by a single PDC cutter under downhole pressurized conditions. Front. Energy Res. 11, 1264804 (2023).
17. Liu, W., Meng, X., Weng, X., Shen, X. & Zhu, X. Rock-breaking performance of specially-shaped PDC cutters from a new insight into the damage beneath cutting groove. Geoenergy Sci. Eng. 231, 212326 (2023).
18. Zhu, X. et al. Rock cutting mechanism of special-shaped PDC cutter in heterogeneous granite formation. J. Pet. Sci. Eng. 210, 110020 (2022).
19. Zhang, Z. et al. Simulation and experimental study on temperature and stress field of full-sized PDC bits in rock breaking process. J. Pet. Sci. Eng. 186, 106679 (2020).
20. Souissi, S., Hamdi, E. & Sellami, H. Microstructure effect on hard rock damage and fracture during indentation process. Geotech. Geol. Eng. 33, 1539-1550 (2015).

21. Huang, H. & Detournay, E. Discrete element modeling of tool-rock interaction II: rock indentation. Int. J. Numer. Anal. Methods Geomech. 37, 1930-1947 (2013).
22. Che, D., Zhu, W.-L. & Ehmann, K. F. Chipping and crushing mechanisms in orthogonal rock cutting. Int. J. Mech. Sci. 119, 224-236 (2016).
23. Xiong, C. et al. Performances of a stinger PDC cutter breaking granite: Cutting force and mechanical specific energy in single cutter tests. Pet. Sci. 20, 1087-1103 (2023).
24. Xiong, C. et al. Comparative analysis cutting characteristics of stinger PDC cutter and conventional PDC cutter. J. Pet. Sci. Eng. 189, 106792 (2020).
25. Xiong, C. et al. Investigations on the Stinger PDC cutter breaking granitoid under in-situ stress and hydrostatic pressure conditions. Int. J. Rock Mech. Min. Sci. 164, 105312 (2023).
26. Xiong, C. et al. 3D cutting force model of a stinger PDC cutter: considering confining pressure and the thermal stress. Rock Mech. Rock Eng. 54, 5001-5022 (2021).
27. Yang, L., Li, Y., Xi, Y., Li, J. & Feng, J. Numerical investigation of rock-breaking mechanisms and influencing factors of different PDC cutters during rotary percussion drilling. Geoenergy Sci. Eng. 241, 213144 (2024).
28. He, W. et al. Numerical simulation of rock-breaking mechanisms by triple-ridged PDC cutter in hard rocks. Geoenergy Sci. Eng. 229, 212148 (2023).
29. Chen, H. et al. Investigation on rock-breaking characteristics of hard sandstone by non-planar PDC cutters under high confining pressure. Geoenergy Sci. Eng. 243, 213268 (2024).
30. Wang, H. et al. Modelling of critical fragment size and rock breaking efficiency evaluation in drilling process. Powder Technol. 469, 121712 (2026).
31. Ding, M., He, M. & Yao, Y. Experimental study of the intrinsic specific energy of water-induced softening rocks under confining pressure condition. Phys. Chem. Earth, Parts A/B/C 142, 104218 (2026).
32. Wang, J., He, M., Wang, H. & Dang, F. Ductile-brittle failure transition of rocks subjected to temperature heating and water cooling in process of drilling with high confining pressure. J. Appl. Geophys. 245, 106037 (2026).
33. Chen, H. et al. Experimental study on conglomerate-breaking mechanism by rotary cutting with triple-ridged PDC cutters and planar PDC cutters. Geoenergy Sci. Eng. 246, 213595 (2025).
34. Dong, Z. et al. A Method for Evaluating the Rock Breaking Efficiency of Cutters and Optimizing the PDC Cutter Profile—A Study of Igneous Rock Formations in Shunbei Oilfield. Energies 15, 6686 (2022).

35. Mandelbrot, B. B., Kol, B. & Aharony, A. Angular gaps in radial diffusion-limited aggregation: two fractal dimensions and nontransient deviations from linear self-similarity. Phys. Rev. Lett. 88, 055501 (2002).

36. Deng, Y., Chen, M., Jin, Y. & Zou, D. Theoretical analysis and experimental research on the energy dissipation of rock crushing based on fractal theory. J. Nat. Gas Sci. Eng. 33, 231-239 (2016).

37. Miao, B., Wang, X. & Li, H. Quantitative analysis of infrared thermal images in rock fractures based on multi-fractal theory. Sustainability 14, 6543 (2022).

38. Li, X. et al. Theoretical study on rock-breaking performances of PDC cutter by fractal characteristics of cutting size. Geoenergy Sci. Eng. 231, 212280 (2023).